Eur. Phys. J. B **11**, 583–591 (1999)

THE EUROPEAN PHYSICAL JOURNAL B

EDP Sciences

Limiting phenomena for the spreading of water on polymer films by electrowetting

M. Vallet, M. Vallade, and B. Berge[a]

Laboratoire de Spectrométrie Physique[b], BP 87, 38402 St Martin d'Hères, France

Received 9 January 1999 and Received in final form 22 January 1999

Abstract. This paper is about fundamental limitations in electrowetting, used as a tool for spreading water solutions on hydrophobic surfaces, like the surface of a polymer film. Up to which point can an electric voltage decrease the contact angle? The first limitation comes when using pure water, above a threshold voltage, little droplets are emitted at the perimeter of the mother drop. We present an analysis of the drop contour line stability, involving competition between electrostatic and capillary forces, which is compatible with observations. The use of salted water solutions suppresses this instability, then one faces a second limitation: the evolution of the contact angle saturates before complete wetting. We show that this saturation is caused by ionisation of the air in the vicinity of the drop edge. We analyse the luminescence induced by gas ionization and measure the related electrical discharges. We explain how air ionization suppresses the driving force for electrowetting and how it induces the formation of an hydrophillic *ring* around the drop.

PACS. 68.45.Gd Wetting – 68.10.Cr Surface energy (surface tension, interface tension, angle of contact, etc.)

1 Introduction

Electrowetting is the control of the wetting properties of a liquid on a solid by the modification of the electric charges present at the solid-liquid interface. Old studies have investigated this effect at electrolyte-mercury [1] or metal-electrolyte interfaces [2,3], but recent research have used the modern engineering of functionnalized surfaces [4–6]. The potential applications belong to microelectronics, microactuators etc. [7–9]. It is now also possible to induce large variations of the contact angle of water solutions on insulating surfaces as polymers, glass or other, using electric fields. The insulator has to be a film and the electrical potential is applied between the water solution and a flat electrode placed on the other side of the film [10,11], as shown in Figure 1. It is possible to explain the variations of contact angle θ by taking into account the stored electrostatic energy, assuming that the capacitance of the drop-film-counter electrode system is given by the simple approximation of the plane infinite capacitor, namely $C = \frac{\epsilon_0 \epsilon}{e} S_{\mathrm{sol-liq}}$. Here ϵ is the dielectric constant of the insulator film, e its thickness and $S_{\mathrm{sol-liq}}$ is the surface of contact of the drop on the film. The electrostatic energy is thus linearly dependent upon the area $S_{\mathrm{sol-liq}}$, which means that this electrostatic energy contributes to modify the interfacial energy of the solid-liquid interface. Consequently, the contact angle θ is expected to vary with the voltage V as:

$$\cos\theta(V) = \cos\theta(0) + \frac{\epsilon_0 \epsilon}{2e\gamma} V^2 \qquad (1)$$

where $\theta(0)$ is the contact angle of the liquid in absence of applied voltage and γ is the liquid surface tension.

In principle one should reach complete wetting when $\cos(\theta) = 1$. Up to now it has never been observed, although the polymer films can withstand very high electric fields: for a 12 μm thick commercial wrapping film, according to equation (1) one expects complete wetting at a voltage of about 160 V, this polymer being able to withstand easily 500 V in the same conditions. What happens instead of going smoothly to complete spreading has been partly already described. For sufficiently pure water, we observed an instability of the drop contour line with droplet expulsion, before complete wetting [11]. The question of the origin of the instability is addressed in this paper. When salt is added in the water, it was shown that the droplet expulsion is suppressed. At some voltage the observed contact angle deviates from the simple prediction of equation (1) and electrowetting saturates. The contact angle saturation might happen abruptly or smoothly, but in all situations reported up to now, namely with various polymers films of different thicknesses from a few μm to about 1 mm using simple water solutions without surfactant, saturation comes for very similar contact angles

[a] e-mail: bruno.berge@ens-lyon.fr
[b] UMR Université Joseph Fourier - CNRS, 5588

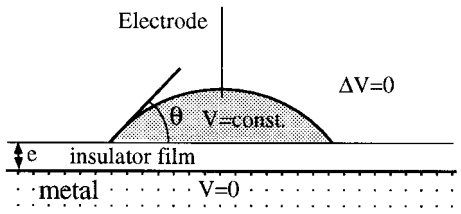

Fig. 1. Schematic side view of the system. A flat infinite electrode is covered with an insulator film of thickness e and dielectric constant ϵ. The drop of conducting liquid (water) is painted in gray: it is equipotential.

in the range $20°-30°$. For high voltages it was shown that the polymer surface becomes hydrophillic around the liquid edge, but outside of the drop.

In this paper we present new quantitative experimental results about the droplet instability and about the saturation phenomenon. We present a linear stability analysis of the contour line at high electric fields, taking into account the excess charges at the drop contour, due to sharp edge electrostatic effects. We also present experimental results about the saturation of the contact angle and a discussion of how the ionization of air through partial discharges can be responsible of this saturation.

2 Experimental results

2.1 Presentation of the problem

Figure 1 presents a side view of the system under study: A drop of water solution (or other conducting liquid) is deposited on a insulator thin solid film (thickness between a few μm and $\simeq 1$ mm). The contact angle of the drop is denoted θ. The reverse side of the polymer is assumed to be grounded by the presence of a conducting surface laterally much larger than the drop.

The derivation of equation (1) is shortly recalled here. The electrostatic energy stored in the capacitor formed by the drop and the counter-electrode is given by

$$E_{\rm elec} = \frac{1}{2}\frac{\epsilon_0\epsilon}{e} S_{\rm sol-liq}\ V^2. \qquad (2)$$

The dependence of $E_{\rm elec}$ with the area $S_{\rm sol-liq}$ means that this electrostatic energy contributes to modify the interfacial energy of the solid-liquid interface, $\gamma_{\rm sol-liq}$:

$$\gamma_{\rm sol-liq}(V) = \gamma_{\rm sol-liq} - \frac{1}{2}\frac{\epsilon_0\epsilon}{e}V^2 \qquad (3)$$

which is formally equivalent to the Lipmann equation $\mathrm{d}\gamma/\mathrm{d}V = \sigma$, where γ is the interface tension, V the potential difference across the interface, and σ the surfacic charge present at one side of the interface. The minus sign comes from the fact that the voltage V is imposed from an external generator. Using Young-Laplace law

$$\cos\theta = \frac{\gamma_{\rm sol-gas} - \gamma_{\rm sol-liq}}{\gamma} \qquad (4)$$

and equation (3) leads to the results of equation (1). If a.c. voltage is applied then V^2 has to be replaced by $V_{\rm eff}^2$ in equations (3, 1).

2.2 experimental details

Polytetrafluoroethylene (PTFE) and High Density Polyethylene (HDPE) films come from Goodfellow, PTFE 13 μm thick were samples from Dupont, polyethylene terephtalate (PET) are a gracious gift from Rhône-Poulenc and we sometimes used silanized glass slides of thickness 0.17 mm or 1 mm. Some experiments were done with kitchen type films, based on poly vinylidene chloride (Albal or Saran). The counter-electrode is a flat stainless steel piece placed under the insulator film. A drop of salted water is placed between the flat electrode and the insulator film, in order to insure a good electrical contact. Usually we used either pure water or water added with Na_2SO_4 at 10^{-2} M/l as the liquid.

The experimental set-up to measure contact angle and to apply high electric voltages has been described previously [11]. We used a Zeiss binocular to observe the sessile drop. In order to look at the weak luminescence around the drop, we equipped the binocular with a sensitive video camera (S.I.T. DAGE-MTI, Michigan-City, Indiana, USA). For detection of the luminescence with even greater sensitivity but without imaging, we used a photomultiplier tube (Hamamatsu R647-04) just above the drop. We used generally a voltage source at 1 kHz. We could measure the partial electric discharges in the air by adding in the circuit of the sample a 1 kΩ resistance which delivers a voltage proportional to the current in the circuit. Discharges are observed either directly with an oscilloscope, or with a high-pass filter to mask the 1 kHz sinusoidal displacement current, as it helps to observe the short pikes, characteristic of partial discharges.

2.3 droplet expulsion

Figure 2 presents contact angle measurements for PTFE films of thickness 50 μm. Three sets of measurements are presented corresponding to three different liquids of different surface tensions: pure water (circles), a 34% ethanol solution in water (triangles) and pure ethanol (squares). For each series a discontinuous line shows the expected values within the simple theory of the infinite plane capacitor, equation (1). The recording stops at the arrow, where emission of droplets occurs. Then the contact angle measurement becomes impossible, due to the perturbation caused by these fastly moving little droplets.

In Figure 3 we show measurements of $\lambda_{\rm c}$ the wavelength of the first unstable mode as a function of the thickness of the insulator film, for a series of measurements made with pure water drops on PTFE films. This is a delicate experiment: when raising the voltage the wetting line moves slowly and stays smooth, but suddenly droplet expulsion starts vigorously. We thus try to capture the average lateral distance between adjacent droplets.

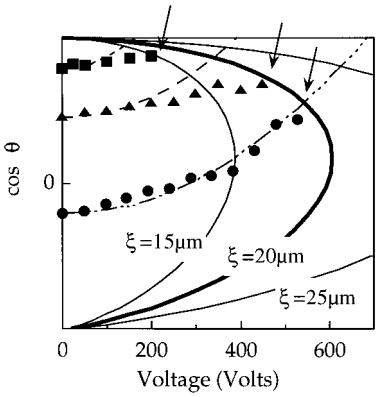

Fig. 2. Experimental values of the contact angle *versus* voltage, for a PTFE film 50 μm thick: pure water (circles), 34% ethanol in water (triangles) and ethanol (squares). For each series, the arrow marks the point where droplet expulsion occurs and the interrupted lines show the theoretical curves in each case, using equation (1). The calculated limit of stability estimated by equation (10) for three different values of the screening length ξ (see text) in the $V - \cos\theta$ plane (continuous lines).

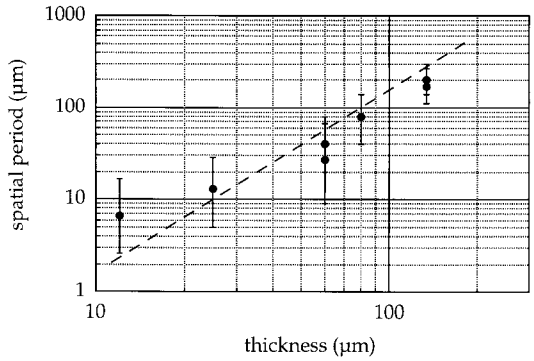

Fig. 3. Log-Log plot of the wavelength (λ_c) of the first unstable mode at the voltage threshold for water droplet emission on teflon films of different thicknesses. It is measured as the mean distance between droplets. The error bar are large because above threshold the droplet are emitted at a high rate and they experience a lot of collisions. The dashed line has a slope 1.

The error bar on this value is large, but the data show unambiguously that there is a correlation between the film thickness and the wavelength λ_c.

2.4 Optical and electrical observation of air ionization near the liquid edge

In this section we look at the case of the spreading of salt solutions by electrowetting. In that case the contact angle variation stops at some voltage, without any sign of instability or droplet ejection. In this section we present the experiments suggesting that saturation is caused by ionization of air around the drop.

Figures 4a and 4b are side views of the drop on a PTFE film 50 μm thick under a voltage of 950 V, chosen above saturation. In Figure 4a there is no external source of light. One sees clearly a luminous ring around the drop of water solution. Figure 4b is the same with a little additional illumination form the rear, in order to observe the spontaneous emission of light and to be able to localize this emission relative to the drop. In this figure it is clear that the spontaneous emission comes from regions outside of the water drop. Figure 5a has been taken also with a little external light, but is viewed from above. Figure 5b shows the pattern observed for a much thinner film, Albal 10 μm thick at $V = 350$ V, exhibiting a clear lateral periodicity in the luminescence, and incomplete ignition of this luminescence around the drop perimeter. When the voltage is set the pattern of luminescence is static, although the intensity usually decreases with time.

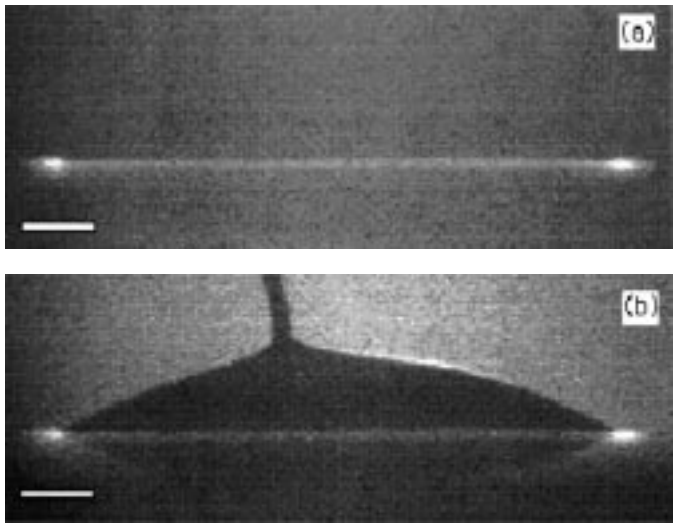

Fig. 4. Visualisation of the luminescence: Side view of the drop on a PTFE film 50 μm thick at $V = 950$ V. This voltage has been chosen above saturation, *i.e.* in the region where the contact angle does not vary anymore with increasing voltage. The bar corresponds to 1 mm. (a) Without external light, (b) with little external light.

Figure 6 shows measurements made for PTFE films, thickness 50 μm. Figure 6a shows the recording during a cycle of the applied voltage and of the emitted light intensity: Light emission in this case starts at a threshold voltage of 500 V. When analysed with an oscilloscope, the light detected is emitted as series of short light pulses. Figure 6b shows, in the same conditions, the number of electric partial discharges per unit time observed as pikes of less than 100 ns duration counted using a scaler. Again there is a threshold voltage for these partial discharges to appear at $\simeq 600$ V. Figure 6c shows the record of the cosine of the contact angle (in fact the average of the advancing and receding contact angle cosines, see [11]) as a function of the applied voltage, showing the deviation of the experimental values from the expectation of equation (1) (continuous line) at a voltage of about 600 V (Curves exhibiting saturation have already been published in Ref. [11], but it is recalled in Fig. 6c). Figure 6 thus shows the approximate concomittance of (i) apparition of luminescent discharges

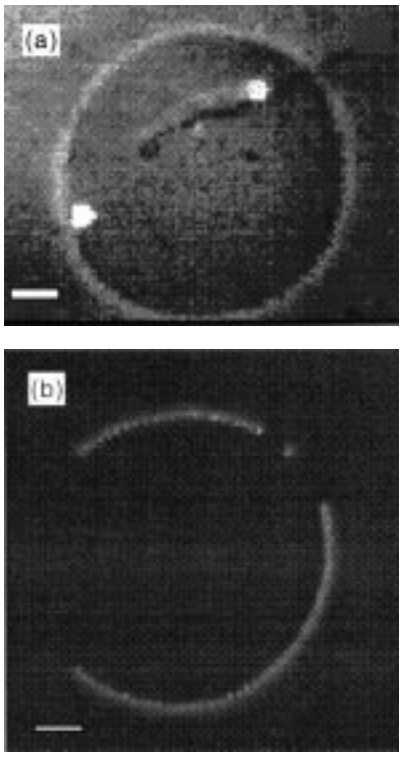

Fig. 5. (a) Visualisation of the luminescence: Top view of the drop on a PTFE film 50 μm thick under 950 V, with little external light. The bar corresponds to 1 mm. (b) Visualisation of the luminescence periodicity: Top view of the drop on a Albal film 10 μm thick under 350 V. The bar corresponds to 1 mm.

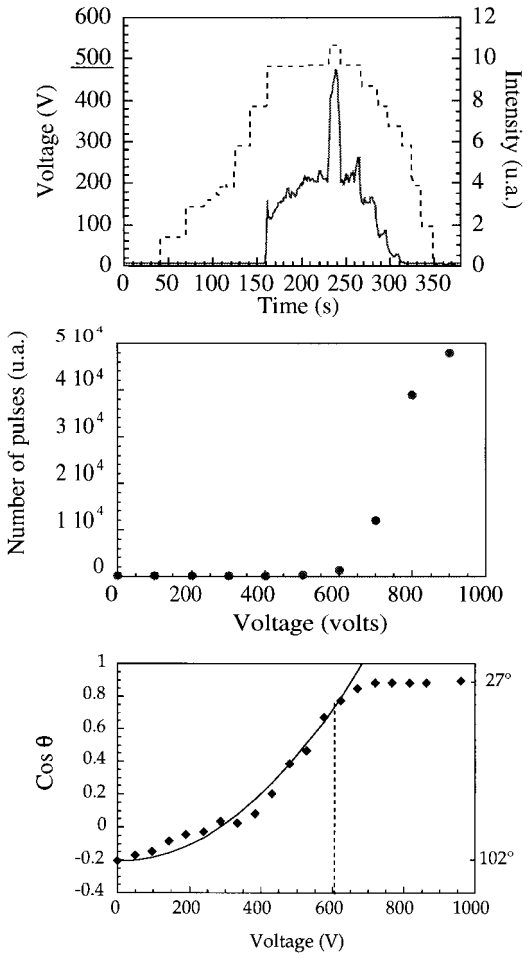

Fig. 6. Three different measurements made on the same film (PTFE, 50 μm), using salted water. (a) Light intensity measured by the photomultiplier (continuous line) and applied voltage (dashed line) as a function of time. (b) Number of partial electric discharges per unit time, as a function of voltage. (c) Cosine of the average of advancing and receding contact angles *versus* voltage.

in the air around the drop, (ii) apparition of electrical pikes in the current, and (iii) saturation of the of contact angle.

We have made the same experiment with different polymer films. We present in Figure 7 the good correlation between the voltage, V_i, where luminescence appears and the saturation voltage, V_s, where contact angle starts to deviate from the variation predicted by the theory. The two last points for rather thick PTFE films are quite inaccurate: due to their stiffness it is difficult to be sure that the polymer film is really applied firmly on the counter-electrode.

We have verified that the light detected by the photomultiplier really comes from the regions outside of the drop, by mounting the photomultiplier on an optical microscope and scanning the drop laterally under the objective. We also made a spectral analysis of the emitted light. Under air atmosphere the major features in the spectra comes from N_2, giving the usual blue-violet luminescence. Under C_2F_6 atmosphere the spectrum was completely changed for *orange* type radiation.

We thus tried to do the same experiment under an SF_6 atmosphere, a better insulator than air, with the hope that saturation could occur at higher voltages. The result was negative, as the saturation of contact angle occurred at about the same voltage. Presumably the good insulator properties of SF_6 are destroyed by trace amounts of water

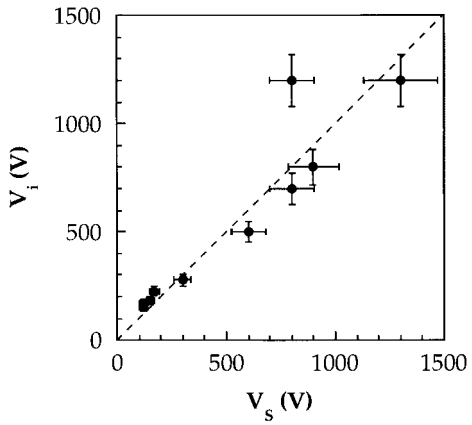

Fig. 7. Saturation voltage, V_s, as a function of the threshold ionisation voltage, V_i. The dark circles are the experimental points, with their estimated error bar. The dashed line represents $V_\mathrm{i} = V_\mathrm{s}$. This picture involves polymer thicknesses ranging from 12 μm to 227 μm.

that are always present in the gas region close to the drop edge.

3 discussion

3.1 Linear stability analysis of the charged wetting line

In this paragraph we go beyond the simple theory found in references [10,11] by taking into account the edge correction to the electrostatic energy $E_{\rm elec}$ stored in the system. $E_{\rm elec}$ is proportional to the electrical capacitance C between the drop and the counter-electrode. The leading term in C is calculated using the infinite plane capacitor formula $C = \frac{\epsilon_0 \epsilon}{e} S$, and is proportional to the surface S of the drop facing the counter-electrode, namely the solid-liquid area. It is known to decrease the effective interfacial energy, under applied voltage [10]. The next term in the capacitance includes a contribution, due to edge corrections, which is proportional to the perimeter L of the basal surface of the drop. This contribution decreases the effective line tension and could be responsible for an instability of the drop contour.

In order to simplify calculations we assumed that the air has the same dielectric constant ϵ than the insulating film, so that the discontinuity at the polymer-air interface (thin continuous line in Fig. 1) disappears from the electrostatic problem. The general problem is then well established. The drop top surface (liquid-gaz) is free to adjust to minimize the *total energy* E of the system:

$$E = \sum_{i=1}^{3} \gamma_i S_i - E_{\rm elec} \tag{5}$$

keeping the drop volume constant. $\sum_{i=1}^{3} \gamma_i S_i$ is the interfacial energy, i denoting the type of interface (liquid-solid liquid-gas or solid-gas) γ_i being the interfacial tension and S_i the area. As usual the minus sign in equation (5) comes from a Legendre transformation to take into account that the drop is maintained at constant voltage by a generator, considered as an outside part of the system. The electrostatic contribution, $E_{\rm elec}$ is given by

$$E_{\rm elec} = \frac{1}{2} C V^2 \tag{6}$$

C, the electrical capacitance, is calculated by solving the Laplacian equation for the electrostatic potential $\Delta v(\mathbf{r}) = 0$ in all space, with the boundary conditions of being zero at the bottom electrode and constant ($v = V$) at the drop surface (see Fig. 1). In Appendix A we present an exact calculation of the capacitance of a 2-D system including edge effects. This leads to the following development for our 3-D system:

$$C \simeq \frac{\epsilon\epsilon_0}{e}\, S + \epsilon\epsilon_0 \left(\frac{1}{\pi - \theta} {\rm Ln} \frac{\sqrt{S}}{e} + A(\theta) \right) L + \ ... \tag{7}$$

where L is the length of the drop perimeter and $A(\theta)$ is a smooth function given in Appendix A (Fig. 9). The first term in equation (7) is the plane infinite capacitor approximation used in Section 2.1 to calculate contact angle variations. The second term is proportional to the perimeter length L and is the leading contribution arising from edge effects.

It is clear that the lineic term will tend to destabilize the drop contour line, because it has the same sign than the surfacic term: for the same reason that the first term in equation (7) leads to a decrease of the surface energy associated to solid-liquid interface, the second term gives a negative contribution to the effective line energy of the drop contour. As expected for macroscopic drops ($L \gg e$) the surfacic term is dominant and the lineic term will not change the equilibrium contact angle.

Using equation (7) one can perform a linear stability analysis of the contact line. One starts from a straight liquid edge which is infinite along the direction of space (y). The liquid wets the solid with a contact angle θ. Now we impose this line to have a sinusoidal perturbation $x = X \cos ky$, where the direction x is in the plane of the solid surface, perpendicular to the three phase contact line. X is the amplitude of the distortion, and k its wave vector.

The distorsion of the wetting line has three main consequences: (i) its length is increased by a factor $\simeq \left(1 + \frac{k^2 X^2}{4}\right)$. (ii) the electric charge distribution close to it is modified. As the length scale relevant for electrostatic edge effects is the thickness e, one expects that the modification of the charge distribution is small when $k \ll 1/e$ and important for $k \gg 1/e$. In the former case the formula for the capacitance of equation (7) is expected to be valid providing one takes into account the increased contour length. In the latter case the roughening of the contour line leads to an electrostatic screening which tends to cancel the effect of its increased length.

As a result of (i) and (ii) the gain in electrostatic energy due to the distortion is estimated to be approximately:

$$\Delta E_{\rm elec} = \frac{\epsilon\epsilon_0}{8} \left(\frac{1}{\pi - \theta} {\rm Ln} \left(\frac{\sqrt{S}}{e} \right) + A(\theta) \right) k^2 {\rm e}^{-k\xi} V^2 X^2 \tag{8}$$

where ξ is a screening length, assumed to be of the order of e. The instability is thus expected to occur for a critical wavevector $k_{\rm c} \simeq 1/\xi$ of the order of $1/e$. This is in rough agreement with observation of the length scale for droplet emission in Figure 3.

(iii) The shape of the drop surface is undulated close to the edge. It is well known that such a deformation dies exponentially with the distance to the edge, with a decay length equal to $1/k$ [13]. Of course for a given amplitude of the line distorsion on the solid surface, X, the surface deformation depends upon θ. The resulting energy cost in surface energy $E_{\rm s}$ per unit length of the line is [14]

$$\Delta E_{\rm s} = \frac{\gamma}{4} k \sin^2\theta\, X^2 \tag{9}$$

where γ is the surface tension of the liquid.

The liquid edge will thus be unstable when the energy gain, equation (8), overcomes the energy cost given by equation (9).

$$\frac{\epsilon\epsilon_0 V^2}{\gamma e} \leq \frac{2}{e k_c \mathrm{e}^{-\xi k_c}} \frac{\sin^2\theta}{\left(\frac{\mathrm{Ln}\frac{\sqrt{S}}{e}}{\pi-\theta} + A(\theta)\right)}. \qquad (10)$$

Figure 2 shows the limit of stability given by equation (10) for a 50 μm Teflon film, in the $V - \cos\theta$ plane, as a continuous line. The drop contour line is expected to be stable on the left side of the line, and unstable on the right side. In order to evaluate numerical values in Figure 2, we have taken $\epsilon = 1.5$, intermediate between the dielectric constants of air and of PTFE (again in this section we neglected the difference), $\mathrm{Ln}\frac{\sqrt{S}}{e} \simeq 4.0$ and $k_c = 2\pi/\lambda_c$ was taken from data shown in Figure 3 ($\lambda_c = 35$ μm).

We can see from Figure 2, that our experimental data can be reasonably accounted for by this model, if the screening length ξ is considered as a fitting parameter. The best agreement is obtained for $\xi \simeq 20$ μm, a length which is of the order of magnitude of the polymer film thickness $e \simeq 50$ μm and of the critical wavelength $\lambda_c \simeq 30-40$ μm. Strictly speaking one should get $\xi = \lambda_c/2\pi \simeq 5-7$ μm which corresponds to the minimum of the right-hand side of equation (10). It is clear however that the present model describes the redistribution of electrostatic charges and screening effects in a very crude way, and one cannot hope it provides an accurate quantitative description of the instability.

The approximate linear dependence of the critical wavelength λ_c with e shown in Figure 3, and the correct order of magnitudes predicted by equation (10) seem to show that the above model of instability contains the right physical ingredients. This could be compared to the so-called *coulomb fission* as it involves only the interplay between capillary and electrostatic forces (see for instance Ref. [15]). Of course a static analysis might not be sufficient, as thin liquid precursor films might be produced at the drop margin. Recent theories show that thin charged liquid films are highly unstable [16].

This paragraph does not explain why the droplet ejection is suppressed when salt is added to the water in mM concentrations, whereas it is maintained when other solutes like ethanol are added even in large quantities. It has probably to do with Marangoni effects but no correct explanation has been produced up to now. In previous works on the spreading of water surfactant mixture [17], Marangoni effects were shown to induce a front instability, but it is conceivable that surface tension gradients stabilize the wetting line.

3.2 Saturation and air ionization

In the case of salted water we believe that the observations presented here show that air ionization is responsible for the contact angle saturation.

First of all, one can understand easily that if the air is ionized, as indicated by the observation of luminescence, electrowetting stops working: the principle of electrowetting is that charges are adsorbed in the conducting liquid at the liquid-solid interface. Due to this adsorption, charges exert a lateral pressure outwards on the wetting line, inducing spreading of the drop. This lateral pressure is exerted on the liquid edge only because air is an insulator, such that charges apply the lateral pressure on the liquid-gas interface, with no possibility of crossing it. If air is ionized, charges can leak from the liquid drop and the lateral pressure builds up less efficiently, weakening the driving force for electrowetting.

The second point is that we observe a concomittance of the threshold voltage for the observation of luminescence and electrical discharges, V_i, with the saturation voltage, V_s, where contact angle deviates from the tendency towards complete wetting (Fig. 7). The concomittance of these voltages, V_i and V_s, has been checked on insulator films of various thicknesses made from very different materials, from glass to PTFE.

As a side effect, we can explain why the surface of the polymer becomes irreversibly hydrophillic on a narrow ring around the drop, but outside of it, as observed in a previous publication [11]. This zone corresponds to a location where the discharges are the most intense, so that they can produce chemical surface modifications similar to corona processing. The consequence is usually to oxidize the surface groups which makes the surface more wettable by water.

The effect of changing the atmosphere from air to SF_6 or C_2F_6 seems to affect the spectrum and intensity of luminescence, but not the saturation voltage at all. We propose that trace amounts of water, at least in the close vicinity of the drop, are enough to decrease considerably the insulating properties of these gases. Nevertheless this point still needs a proof. We should note that in some cases, like in Figure 5b, one observes a lateral periodicity in the pattern of the luminescence: we cannot exclude that the sinusoidal instability described in the preceding section happens without leading to droplet emission, such that the luminescence reveals an underlying geometric distorsion of the contour line, otherwise undetectable.

The following question is interesting: Why do the contact angle variation stop always at about the same value of the contact angle, *i.e.* 20°-30°? What is special with this value? Within the infinite plane capacitor approximation equation (1), it means that in our experiments saturation occurs at approximately constant V^2/e values, whatever the thickness and the nature of the dielectric film. Ignition of the ionization depends actually on the electric field near the edge of the drop, which is large due to sharp edge effects. This field is difficult to calculate exactly [18] because it depends on the precise shape of the drop surface. For a 2D model of a rounded drop edge the electric field is calculated using conformal mapping methods in Appendix B. Its maximal value E_{max} is found to be equal to $V/\sqrt{\pi e\rho}$, where ρ is the radius of curvature at the liquid edge. Attempts to measure optically the rounding of the drop surface at its margin failed. Nevertheless if one assumes that ρ is small and constant, then it could explain

the experimental observations that V^2/e is roughly constant at saturation. It is reasonable to assume that ρ is a microscopic length which is related to the properties of water (possibly to the debye length) such that the rounding of the edge is not detectable by optical microscopy.

4 Conclusion

We have shown in this paper that one can account for the instability of the drop, observed for pure water or water-ethanol mixtures, by a simple analysis involving the competition between electrostatic and capillary forces. The prediction of threshold voltage of instability corresponds to the experimental measurements, if one considers a screening length ξ of the order of 20 μm for an insulator thickness of $e = 50$ μm. The expectation that the wave vector of the most unstable mode is proportional to the insulator thickness, is roughly observed.

Addition of salt to the water suppresses the instability, for unknown reasons. In that case we show that air ionization is responsible for the saturation of the contact angle with increasing voltage. The threshold voltage where ionization starts coincides with the voltage at which electrowetting begins to loose its efficiency, as shown by the discrepancy between observed contact angles and values predicted by equation (1). Nevertheless the value of threshold voltage where ionization starts is not explained: a better understanding of these phenomena requires the resolution of a rather difficult electrostatic problem with free boundary (the drop surface) and singularities at the three phase contact line.

We address a special thank to Pr. Pierre Atten (Univ. Grenoble) for his suggestion of looking at electrical discharges. We thank Dr. Filippini for fruitful discussions. We also had a very efficient support from Sonia Letant and J. Derouard, who made possible the spectral analysis of the luminescence. We had many useful discussions with Pr Jo Lajzerowicz (Univ. Grenoble).

Note added in proof

Note that the saturation of the contact angle has been also observed in the following reference: W.J.J. Welters, L.G. Fokkink, Langmuir **14**, 1535 (1998).

Appendix A: Sharp edge effects

The capacitance of the 2-dimensional electrostatic system shown in Figure 8 can be calculated using conformal mapping methods. As described in reference [19] the electrostatic properties of this system can be obtained from the Schwarz-Christofell formula:

$$Z(w) = \int_{\mathrm{i}\pi}^{w} (\mathrm{e}^{w'} + 1)^{\alpha} \mathrm{d}w' + \mathrm{i}\pi \tag{11}$$

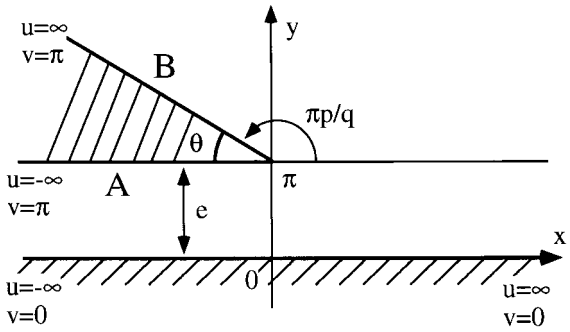

Fig. 8. Model used to calculate the edge contribution to the capacitance.

where $Z = x + \mathrm{i}y$ and $w = u + \mathrm{i}v$ are the complex coordinates of the mapping (in units of e/π and V/π respectively) and α is related to the contact angle θ of the drop: $\theta = (1 - \alpha)\pi$.

The integral (11) can be explicitly calculated when α is a rational number: $\alpha = p/q$ (p, q positive integers). Putting $\zeta = (\mathrm{e}^{w} + 1)^{1/q}$ ($0 \leq \mathrm{Arg}(\zeta) \leq \pi/q$) one gets:

$$Z(w) - \mathrm{i}\pi = \frac{q}{p}\zeta^p + \sum_{j=0}^{q-1} \mathrm{e}^{2\mathrm{i}\pi jp/q} \mathrm{Ln}(1 - \mathrm{e}^{-2\mathrm{i}\pi j/q}\ \zeta). \tag{12}$$

One can easily check that the special cases $\theta = 0$ ($p/q = 1$) and $\theta = \pi/2$ ($p/q = 1/2$) correspond respectively to

$$Z(w) = \mathrm{e}^{w} + 1 + w \tag{13}$$

and

$$Z(w) = 2\sqrt{\mathrm{e}^{w} + 1} + 2\mathrm{Ln}(\sqrt{\mathrm{e}^{w} + 1} - 1) - w \tag{14}$$

in agreement with the results found by Lavrentiev *et al.* in reference [19], p. 189. The equipotential lines are parametrized by u at constant v.

On the upper electrode: $v = \pi$. For $u \leq 0$, $\zeta = (1 - \mathrm{e}^{u})^{1/q} \leq 1$ and:

$$\begin{cases} x(u) = \dfrac{q}{p}\zeta^p + \displaystyle\sum_{j=0}^{q-1} \mathrm{e}^{2\mathrm{i}\pi jp/q} \mathrm{Ln}(1 - \mathrm{e}^{-2\mathrm{i}\pi j/q}\ \zeta) \\ y(u) = \pi. \end{cases} \tag{15}$$

This corresponds to the part A of the electrode in Figure 8. For $u \geq 0$, $\zeta = (\mathrm{e}^{u} - 1)^{1/q}\mathrm{e}^{\mathrm{i}\pi/q}$ and:

$$\begin{cases} x(u) = \left[\dfrac{q}{p}\,|\zeta|^p + \displaystyle\sum_{j=0}^{q-1} \mathrm{e}^{2\mathrm{i}\pi(j-1/2)p/q} \right. \\ \qquad \left. \times \mathrm{Ln}(1 - \mathrm{e}^{-2\mathrm{i}\pi(j-1/2)/q}\ |\zeta|)\right] \cos\dfrac{\pi p}{q} \\ y(u) = \pi + \left[\dfrac{q}{p}\,|\zeta|^p + \displaystyle\sum_{j=0}^{q-1} \mathrm{e}^{2\mathrm{i}\pi(j-1/2)p/q} \right. \\ \qquad \left. \times \mathrm{Ln}(1 - \mathrm{e}^{-2\mathrm{i}\pi(j-1/2)/q}\ |\zeta|)\right] \sin\dfrac{\pi p}{q}. \end{cases} \tag{16}$$

This corresponds to the part B of the electrode in Figure 8. On the lower electrode $v = 0$ so that $\zeta = (\mathrm{e}^u + 1)^{1/q} \geq 1$ and:

$$\begin{cases} x(u) = \frac{q}{p}\zeta^p + \mathrm{Ln}(\zeta - 1) + \sum_{j=1}^{q-1} \mathrm{e}^{2\mathrm{i}\pi jp/q \mathrm{Ln}(1-\mathrm{e}^{-2\mathrm{i}\pi j/q}\zeta)} \\ y(u) = 0 \end{cases} \tag{17}$$

the charge density σ on the electrodes is related to the electric field $\mathbf{E}$ near these electrodes and is given by:

$$|\sigma| = \epsilon_0 \left| E_x - \mathrm{i}E_y \right| = \frac{\epsilon_0 V}{e} \left| \frac{\mathrm{i}}{\mathrm{d}Z/\mathrm{d}w} \right| = \frac{\epsilon_0 V}{e} \frac{1}{(\mathrm{e}^w + 1)^\alpha} \cdot \tag{18}$$

On the part A of the upper electrode one has:

$$|\sigma| = \frac{\epsilon_0 V}{e} \frac{1}{(1 - \mathrm{e}^u)^\alpha} \tag{19}$$

taking into account equation (15) one finds that $|\sigma| = \frac{\epsilon_0 V}{e}$ far from the edge and it diverges near the edge according to:

$$|\sigma| \simeq \frac{\epsilon_0 V}{e} \frac{1}{(\alpha + 1)^\alpha} \left(\frac{e}{\pi |x|} \right)^{\frac{\alpha}{\alpha+1}} \cdot \tag{20}$$

This divergence is most important for small θ ($\sigma \simeq |x|^{-1/2}$) and it disappears, as expected, for $\theta = \pi$. On the lower electrode one has:

$$|\sigma| = \frac{\epsilon_0 V}{e} \frac{1}{(1 + \mathrm{e}^u)^\alpha} \cdot \tag{21}$$

Taking into account equation (17) this charge density is found to be $|\sigma| = \epsilon_0 V/e$ for $x \to -\infty$ and $|\sigma| = \frac{\epsilon_0 V}{\pi - \theta} \frac{1}{|x|}$ for $x \to \infty$. The total charge Q on the lower electrode between x_1 and x_2 is simply given by:

$$|Q| = \int_{x_1}^{x_2} |\sigma| \, \mathrm{d}x = \frac{\epsilon_0 V}{\pi} (|u(x_2)| - |u(x_1)|). \tag{22}$$

For $(-x_1/e) \gg 1$ and $(x_2/e) \gg 1$ one gets:

$$|Q| = \frac{\epsilon_0 V}{\pi} \left(\frac{|x_1|}{e} + \frac{1}{\pi - \theta} \mathrm{Ln} \left((\pi - \theta) \frac{x_2}{e} \right) + A(\theta) \right) \tag{23}$$

where $A(\theta)$ is given by:

$$A(\theta) = \frac{p}{q} + \sum_{j=1}^{q-1} \mathrm{e}^{2\mathrm{i}\pi jp/q} \mathrm{Ln} \left(1 - \mathrm{e}^{-2\mathrm{i}\pi j/q} \right) - \mathrm{Ln}(q). \tag{24}$$

Although not obvious, this expression actually depends only on p/q, (*i.e.* on θ) and it decreases monotonically from 1 at $\theta = 0$ to 0 at $\theta = \pi$ (it is related to the edge effect). The numerical function $A(\theta)$ has been evaluated and is shown in Figure 9.

The capacitance of the 2-dimensional system is then for $|x_1| \simeq x_2 \simeq R$

$$C = \epsilon_0 \left(\frac{R}{e} + \frac{1}{\pi - \theta} \mathrm{Ln} \left(\frac{(\pi - \theta) R}{e} \right) + A(\theta) \right). \tag{25}$$

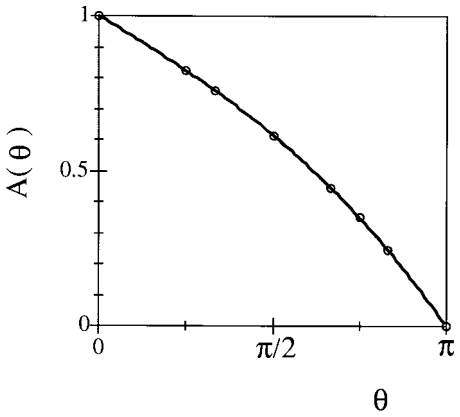

Fig. 9. Graph of the function A defined in equation (24) *versus* the contact angle θ

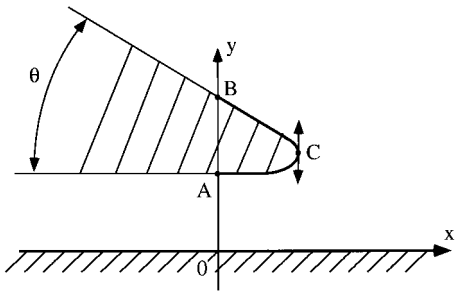

Fig. 10. Model of the rounded edge drop.

Appendix B: Rounded edge

In order to find an estimation of the maximum electric field value near the edge one has to consider a rounded edge as shown in Figure 10. As discussed in reference [19] the electrostatic problem of rounded edge systems can be solved using the conformal mapping defined by:

$$Z(w) = \frac{1}{1+\gamma} \int_{\mathrm{i}\pi}^{w} \left[(\mathrm{e}^{w'} + 1)^\alpha + \gamma (\mathrm{e}^{w'} + 1 + \beta)^\alpha \right] \mathrm{d}w' + \mathrm{i}\pi \tag{26}$$

the constants $\beta \ll 1$ and γ determined the rounding of the edge. Near the edge, for $0 < u \ll 1$ and $v = \pi$, equation (26) leads to:

$$Z(w) = \mathrm{i}\pi + \frac{1}{(1+\gamma)(1+\alpha)} \times \left[\mathrm{e}^{\mathrm{i}\pi\alpha} u^{\alpha+1} - \gamma \left[(\beta - u)^{\alpha+1} - \beta^{\alpha+1} \right] \right]. \tag{27}$$

As the actual shape of the drop edge is not known, one has to make some rather arbitrary assumption. Let us choose the point B defined by $u = \beta$ to be at $x = 0$:

$$x_\mathrm{B} = \frac{\beta^{\alpha+1}}{(1+\gamma)(1+\alpha)} (-\cos(\theta) + \gamma) = 0 \implies \gamma = \cos(\theta) \tag{28}$$

$$y_\mathrm{B} = \pi + \frac{\beta^{\alpha+1}}{(1+\alpha)} \mathrm{tg} \frac{\theta}{2} \cdot \tag{29}$$

Let us define the point C by $u = \beta/2$ its coordinates are:

$$x_{\mathrm{C}} = \frac{\beta^{\alpha+1}}{1+\alpha}\frac{\cos(\theta)}{1+\cos(\theta)}(1-2^{-\alpha}) \tag{30}$$

$$y_{\mathrm{C}} = \pi + \frac{1}{1+\alpha}\left(\frac{\beta}{2}\right)^{\alpha+1}\mathrm{tg}\frac{\theta}{2}\cdot \tag{31}$$

The electric field near the edge is given by:

$$\begin{aligned} E_x - \mathrm{i}E_y &= \frac{V}{e}\left[\frac{\mathrm{i}(1+\gamma)}{(\mathrm{e}^w+1)^\alpha + \gamma(\mathrm{e}^w+1+\beta)^\alpha}\right] \\ &\simeq \frac{V}{e}\left[\frac{\mathrm{i}(1-\cos\pi\alpha)}{\mathrm{e}^{\mathrm{i}\pi\alpha}u^\alpha - \cos\pi\alpha\ (\beta-u)^\alpha}\right]. \end{aligned} \tag{32}$$

Near the point C, one then finds that:

$$\begin{cases} E_x = \dfrac{V}{e}\left(\dfrac{\beta}{2}\right)^{-\alpha}\mathrm{cotg}\dfrac{\theta}{2} \\ E_y = 0. \end{cases} \tag{33}$$

This shows that the rounded edge has a vertical tangent at C. The radius of curvature ρ at C is given by:

$$\rho = \frac{e}{\pi}\left(\frac{\mathrm{d}^2x}{\mathrm{d}y^2}\right)^{-1} = \frac{e}{2\pi\alpha}\left(\frac{\beta}{2}\right)^{\alpha+1}\mathrm{tg}\,\theta\ \mathrm{tg}\frac{\theta}{2}\cdot \tag{34}$$

The electric field near C is thus of the form:

$$E_{\mathrm{c}} = \frac{V}{e}\left(\frac{e\ \mathrm{tg}\,\theta}{2\pi\alpha\rho}\right)^{\frac{\alpha}{\alpha+1}}\left(\mathrm{tg}\frac{\theta}{2}\right)^{\frac{-1}{\alpha+1}}\cdot \tag{35}$$

For small θ, $\alpha \simeq 1$ and one has:

$$E_{\mathrm{c}} \simeq \frac{V}{\sqrt{\pi e\rho}}\cdot \tag{36}$$

This field is expected to correspond to the maximum electric field near the edge in the present model.

References

1. G. Lippmann, Anal. Chim. **48**, 776 (1886).
2. D.C. Grahame, Chem. Rev. **41**, 441 (1947).
3. A. Froumkine, Actual. Sci. **373**, (1936).
4. J.A.M. Sondag-Huethorst, L.G.J. Fokkink, J. Electroanal. Chem. **367**, 49 (1994), and references cited therein.
5. J.A.M. Sondag-Huethorst, L.G.J. Fokkink, Langmuir **10**, 4380 (1994). See also J.A.M. Sondag-Huethorst, Thesis 1994 (CIP-Gegevens Koninklijke Bibliotheek, den Haag, the Netherlands).
6. N.L. Abbott, G.M. Whitesides, Langmuir **10**, 1493 (1994).
7. E. Colgate, H. Matsumoto, J. Vac. Sci. Technol. A **8**, 4 (1990).
8. J.L. Jackel, S. Hackwood, J.J. Veselka, G. Beni, Appl. Opt. **22**, 1765 (1983), and references cited therein.
9. M. Sato, IEICE Trans. Commun. **E77-B**, 197 (1994).
10. B. Berge, C.R. Acad. Sci. Paris Sér. II **317**, 157 (1993).
11. M. Vallet, L. Vovelle, B. Berge, Polymer **37**, 2465 (1996).
12. L. Landau, E. Lifchitz, *Électrodynamique des milieux continus* (Éditions Mir, Moscou, 1969).
13. J.F. Joanny, P.G. de Gennes, J. Chem. Phys. **81**, 552 (1984).
14. M.O. Robbins, J.F. Joanny, Europhys. Lett. **3**, 729 (1987).
15. A. Gomez, K. Tang, Phys. Fluids **6**, 404 (1994).
16. A.I. Grigor'ev, M.I. Munichev, S.O. Shiryaeva, J. Colloid Interface Sci. **166**, 267 (1994).
17. S.M. Troian, E. Herbolzheimer, S.A. Safran, Phys. Rev. Lett. **65**, 333 (1990) and references cited therein.
18. Solving the 3D "free boundary" problem with singularities is a very difficult task. An interesting attempt has been conducted in the following reference: S. Bouchereau, Thèse de l'Université de Grenoble (1997), unpublished.
19. M. Lavrentiev, B. Chabat, *Méthodes de la théorie des fonctions d'une variable complexe* (Éditions MIR, Moscou, 1977).